Numerical Heat Transfer, Part A, 43: 239–258, 2003

1040-7782/03 $12.00 + .00
DOI: 10.1080/10407780390122655

Taylor & Francis
Taylor & Francis Group

HEAT TRANSFER AND HYDROMAGNETIC CONTROL OF FLOW EXIT CONDITIONS INSIDE OSCILLATORY SQUEEZED THIN FILMS

A.-R. A. Khaled
Department of Mechanical Engineering, The Ohio State University, Columbus, Ohio, USA

K. Vafai
Department of Mechanical Engineering, University of California, Riverside, California, USA

The influence of fluids inertia and the effects of the presence of a magnetic field normal to the direction of the flow of an electrically conducting fluid are studied on flow and heat transfer inside a nonisothermal and incompressible thin film undergoing oscillatory squeezing. The governing equations have been nondimensionalized and solved numerically. Further, the influence of the squeezing Reynolds number, thermal squeezing number, Hartmann number, and the squeezing frequency are determined. It is shown that flow instabilities appear at large squeezing Reynolds numbers and that the Nusselt number is affected by inertia effects as a result of increased squeezing Reynolds number. Further, it is found that flow instabilities are reduced when the magnetic field is introduced.

INTRODUCTION

Flow and heat transfer inside thin films has received a lot of attention in recent years because it is widely used in engineering applications such as in lubrication, heat pipes, and microchannels. In certain applications, external disturbances such as unbalances in rotating machines and increased noise levels from the surroundings can result in an oscillatory motion at the boundary. Even small oscillating motion can have a substantial impact, as the thickness of thin films is very small. Accordingly, the dynamics and thermal characterization of thin films will be altered.

The chambers for chemical and biological detection systems such as fluidic cells for chemical or biological microcantilever probes (Lavrik et al. [1]) are an important example for thin films. Small turbulence levels that can be introduced into these cells by either flow pulsating at the inlet or external noise that may be present at the boundaries, which results in a vibrating boundary, can produce flow instabilities inside the fluidic cells. These disturbances have large influence on the measurements

Received 21 March 2002; accepted 29 April 2002.
Address correspondence to Professor K. Vafai, Dept. of Mechanical Engineering, University of California, Riverside, A363 Bourns Hall, Riverside, CA 92521-0425. E-mail: vafai@engr.ucr.edu

NOMENCLATURE

B	thin film length	x	x-coordinate
B_m	magnetic field strength	X	dimensionless x-coordinate
c_p	specific heat of the fluid	y	y-coordinate
H	dimensionless thin film thickness	Y	dimensionless y-coordinate
Ha	Hartmann number	Ω	vorticity
h	thin film thickness	Ω^*	dimensionless vorticity
h_c	convective heat transfer coefficient at the lower plate	Ψ	stream function
		Ψ^*	dimensionless stream function
h_0	reference thin film thickness	β	dimensionless squeezing motion amplitude
k	thermal conductivity of the fluid		
Nu_L	local Nusselt number at the lower wall	ε	perturbation parameter
Pr	Prandtl number	γ	dimensionless frequency
P_S	thermal squeezing parameter	η	variable transformation for Y-coordinate
p	fluid pressure	μ	dynamic viscosity of the fluid
q_0	heat flux at the lower plate	θ	dimensionless temperature in flow field
R_L	lateral Reynolds number	θ_m	dimensionless mean bulk temperature
R_S	squeezing Reynolds number	ρ	density of the fluid
t	time	σ	squeezing number
T	temperature in fluid	σ_m	electrical conductivity of the fluid
T_1	inlet fluid temperature	τ	dimensionless time
T_m	mean bulk temperature	υ	kinematic viscosity
U	dimensionless velocity in the x-direction	ω	reciprocal of a reference time (reference squeezing frequency)
u	velocity in the x-direction		
v	velocity in the y-direction	ξ	variable transformation for the dimensionless x-coordinate
V	dimensionless velocity in the y-direction		

of the biological probes, especially those utilizing microcantilevers, as these detecting elements are very sensitive to flow conditions. Therefore, a special design for these fluidic cells is needed in order to transport the target proteins to the probes with minimum effects of turbulence or thermal disturbances.

Many researchers have analyzed flow in hydrodynamic or squeezed thin films like Langlois [2], who solved analytically hydrodynamic pressure in isothermal squeezed films with fluid density varying according to the pressure. Later, toward the end of the twentieth century, interest in studying flow inside squeezed thin films increased. For example, Damodaran et al. [3] considered the effect of a moving boundary on pulsatile flow of incompressible fluid. Further, Bhattacharjee et al. [4] analyzed the flow of dusty fluids inside squeezed thin films. To the authors' best knowledge there are very few studies that considered heat transfer inside squeezed thin films.

Among those studies that considered effects of squeezing on the temperature distribution inside the thin film are those of Hamza [5] and Bhattacharyya et al. [6]. Although they considered thermal aspects in their analysis, their work addressed other aspects not considered in this work. For example, Hamza [5] considered the external squeezing velocity to have a certain function in order to have similarity solutions, and he also assumed that temperature is only a function of the coordinate normal to the axis of the thin film. Bhattacharyya et al. [6] considered a constant squeezing velocity at one boundary; they assumed also that the temperature field is one dimensional. Moreover, both works were concerned with flow between two

parallel disks, and this simplified their flow formulations as the reduced transformed momentum equations tended to be one dimensional.

Recently, Debbaut [7] considered in his work the influence of external squeezing on temperature distribution inside thin films. However, in his analysis he considered a constant squeezing velocity and a fixed volume of squeezed fluid. Later on, Khaled and Vafai [8] considered heat transfer in incompressible squeezed thin films with sinusoidal squeezing, but they did not include the inertia effects.

In the literature, Chamkha [9], among many others, considered the effects of the presence of a magnetic field on the flow and heat transfer inside channels, yet few of them, including Bhattacharyya and Pal [10], considered the applications of a magnetic field inside squeezed thin films. As such, the magnetic field effects on both flow and heat transfer are discussed in this study.

Here we transform into dimensionless forms the vorticity-stream function formulation and the energy equation for a thin film with its upper plate having oscillatory motion. The transformed equations have been solved numerically, and the influence of squeezing Reynolds number, Hartmann number, and squeezing frequency are determined on both flow and heat transfer characteristics inside the thin film.

PROBLEM FORMULATION

Consider a two-dimensional thin film that has a small thickness h compared with its length B. The x-axis is taken in the direction of the length of the thin film, while the y-axis is taken along the thickness as shown in Figure 1. The lower plate of the thin film is fixed, while the vertical motion of the upper plate is assumed to have sinusoidal behavior according to the following relation:

$$h = h_o(1 - \beta \cos(\gamma \omega t)) \tag{1}$$

where h_o, β, and ω are the reference thin film thickness, upper plate motion amplitude, and a reference frequency, respectively. γ is the dimensionless frequency. It is assumed that the fluid is Newtonian and has constant properties. Further, the fluid is

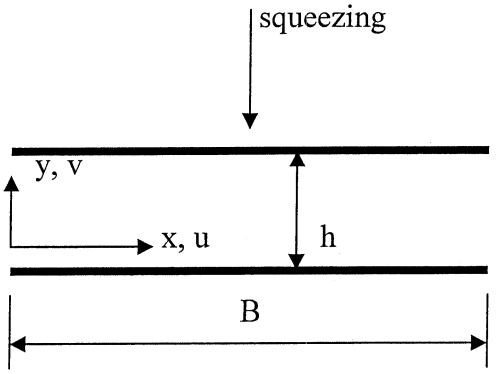

Figure 1. Schematic diagram.

assumed to be electrically conducting and that the magnetic Reynolds number is very small so that the induced magnetic field and the Hall effect of magnetohydrodynamics are negligible.

General Model

The general two-dimensional continuity, momentum, and energy equations, including magnetic field effects for the laminar thin film, are given as

$$\frac{\partial u}{\partial x}+\frac{\partial v}{\partial y}=0 \tag{2}$$

$$\rho\left(\frac{\partial u}{\partial t}+u\frac{\partial u}{\partial x}+v\frac{\partial u}{\partial y}\right)=-\frac{\partial p}{\partial x}+\mu\left(\frac{\partial^2 u}{\partial x^2}+\frac{\partial^2 u}{\partial y^2}\right)-\sigma_m \mathrm{B}_m^2 \mathrm{u} \tag{3}$$

$$\rho\left(\frac{\partial v}{\partial t}+u\frac{\partial v}{\partial x}+v\frac{\partial v}{\partial y}\right)=-\frac{\partial p}{\partial y}+\mu\left(\frac{\partial^2 v}{\partial x^2}+\frac{\partial^2 v}{\partial y^2}\right) \tag{4}$$

$$\rho c_p\left(\frac{\partial T}{\partial t}+u\frac{\partial T}{\partial x}+v\frac{\partial T}{\partial y}\right)=k\left(\frac{\partial^2 T}{\partial x^2}+\frac{\partial^2 T}{\partial y^2}\right) \tag{5}$$

where T, ρ, p, μ, c_p, and k are the fluid temperature, density, pressure, dynamic viscosity, specific heat, and the thermal conductivity of the fluid, respectively. Further, σ_m and B_m are the electric conductivity of the fluid and the applied magnetic field strength normal to the flow of the fluid inside the flat thin film, respectively.

It is convenient to transform Eqs. (2) through (4) to vorticity stream function formulations for cases with large inertia effects. These equations are listed below in dimensional form:

$$\frac{\partial \Omega}{\partial t}+u\frac{\partial \Omega}{\partial x}+v\frac{\partial \Omega}{\partial y}=\upsilon\left(\frac{\partial^2 \Omega}{\partial x^2}+\frac{\partial^2 \Omega}{\partial y^2}\right)+\frac{\sigma_m B_m^2}{\rho}\frac{\partial u}{\partial y} \tag{6}$$

$$\frac{\partial^2 \Psi}{\partial x^2}+\frac{\partial^2 \Psi}{\partial y^2}=-\Omega \tag{7}$$

where Ω and Ψ are the dimensional vorticity and stream functions, respectively. The vorticity and stream functions are related to the velocity components through the following:

$$\Omega=\frac{\partial v}{\partial x}-\frac{\partial u}{\partial y} \tag{8}$$

$$u=\frac{\partial \Psi}{\partial y} \qquad v=-\frac{\partial \Psi}{\partial x} \tag{9a, b}$$

Equation (6) can be approximated as the following for thin films:

$$\frac{\partial\Omega}{\partial t}+u\frac{\partial\Omega}{\partial x}+v\frac{\partial\Omega}{\partial y}=\upsilon\left(\frac{\partial^2\Omega}{\partial x^2}+\frac{\partial^2\Omega}{\partial y^2}\right)-\frac{\sigma_m B_m^2}{\rho}\Omega \tag{10}$$

This is because the last term in Eq. (6), $\partial u/\partial y$, has a higher order of magnitude than $\partial v/\partial x$. Therefore, it can be approximated by the negative of the vorticity Ω.

Boundary Conditions

The dimensional boundary conditions for this problem are listed below:

$$\begin{aligned}
&\Psi(0,y,t)=V_o y \qquad \frac{\partial^2\Psi(B,y,t)}{\partial x^2}=0\\
&\Psi(x,0,t)=0 \qquad \Psi(x,h,t)=V_o h-h_o\omega x\beta\gamma\sin(\gamma\omega t)\\
&\Psi(x,y,0)=0\\
&u(0,y,t)=V_o \quad u(x,0,t)=0 \quad u(x,h,t)=0\\
&v(x,0,t)=0 \qquad v(x,h,t)=h_o\omega\gamma\beta\sin(\gamma\omega t)
\end{aligned} \tag{11}$$

$$\begin{aligned}
&\Omega(0,y,t)=-\varepsilon^2\frac{\partial^2\Psi(0,y,t)}{\partial x^2} \qquad \frac{\partial^2\Omega(B,y,t)}{\partial x^2}\cong 0\\
&\Omega(x,0,t)=-\frac{\partial u(x,0,t)}{\partial y} \qquad \Omega(x,h,t)=-\frac{\partial u(x,h,t)}{\partial y}
\end{aligned} \tag{12}$$

$$\begin{aligned}
&T(x,y,0)=T_1 \quad T(0,y,t)=T_1 \quad -k\frac{\partial T(x,0,t)}{\partial y}=q_0 \quad \frac{\partial T(x,h,t)}{\partial y}=0\\
&\frac{\partial T(B,y,t)}{\partial x}=\frac{q_0}{\rho c_p u_m(B,t)h(B,t)}-\frac{1}{u_m(B,t)}\frac{\partial T_m(B,t)}{\partial t}
\end{aligned} \tag{13}$$

where T_1 is the inlet and initial temperatures. q_o is a constant representing the heat flux prescribed at the lower plate, whereas the upper plate is assumed insulated. It is assumed in Eqs. (11) that the fluid inside the thin film is initially at rest and for $t>0$ the inlet velocity is kept constant, which is equal to V_o. The axial gradient of the normal component of the velocity is considered zero at the exit. Further, the lower plate is fixed and is assumed to have zero value for the stream function. Accordingly, the stream function at the upper plate includes the inlet flow rate as well as the flow rate induced by the motion of the upper plate. Note that this flow has linear distribution, with x as predicted from the continuity equation. Accordingly, Eq. (7) suggests that the exit condition for the dimensionless vorticity can be approximated by the second condition in Eqs. (12).

The thermal boundary conditions and the initial condition are found in Eqs. (13). The exit condition is derived using an integral energy balance. When the energy balance is applied, axial conduction is assumed negligible at the exit, and the axial gradient of the mean temperature at the exit is taken to be similar to axial

gradients of temperatures there. For highly convective applications, the axial diffusive terms appearing in Eqs. (5) and (6) can be neglected. Therefore, solutions to these equations will be less dependent on the exit conditions. The terms u_m and T_m, defined below, are the exit average axial velocity and the exit mean bulk temperature, respectively:

$$T_m(x,t) = \frac{1}{u_m(x,t)h}\int_o^h u(x,y,t)T(x,y,t)dy \tag{14}$$

Dimensionless Governing Equations

The following set of dimensionless variables is suggested:

$$X = \frac{x}{B} \qquad Y = \frac{y}{h_o} \tag{15a,b}$$

$$\tau = \omega t \tag{15c}$$

$$\Omega^* = \frac{\Omega}{(V_o + \omega B)/h_o} \qquad \Psi^* = \frac{\Psi}{h_o(V_o + \omega B)} \tag{15d,e}$$

$$\theta = \frac{T - T_1}{(q_o h_o)/k} \tag{15f}$$

where Ω^* and Ψ^* are the corresponding dimensionless values of Ω and Ψ, respectively. The introduction of variable (15*e*) in Eqs. (9*a*, *b*) results in the following dimensionless velocity components:

$$U = \frac{u}{V_o + \omega B} \qquad V = \frac{v}{\varepsilon(V_o + \omega B)} \tag{16a,b}$$

The dimensionless vorticity-stream function formulations for the flow inside the thin film and the dimensionless energy equation are

$$R_S\frac{\partial\Omega^*}{\partial\tau} + (R_S + R_L)\left(\frac{\partial\Psi^*}{\partial Y}\frac{\partial\Omega^*}{\partial X} - \frac{\partial\Psi^*}{\partial X}\frac{\partial\Omega^*}{\partial Y}\right) = \left(\varepsilon^2\frac{\partial^2\Omega^*}{\partial X^2} + \frac{\partial^2\Omega^*}{\partial Y^2}\right) - H_a^2\Omega^* \tag{17}$$

$$\left(\varepsilon^2\frac{\partial^2\Psi^*}{\partial X^2} + \frac{\partial^2\Psi^*}{\partial Y^2}\right) = -\Omega^* \tag{18}$$

$$P_s\left(\frac{\partial\theta}{\partial\tau} + \left(1 + \frac{R_L}{R_S}\right)\left(\frac{\partial\Psi^*}{\partial Y}\frac{\partial\theta}{\partial X} - \frac{\partial\Psi^*}{\partial X}\frac{\partial\theta}{\partial Y}\right)\right) = \varepsilon^2\frac{\partial^2\theta}{\partial X^2} + \frac{\partial^2\theta}{\partial Y^2} \tag{19}$$

where $\varepsilon = h_o/B$. Further, R_S, R_L, P_S and Ha are the squeezing Reynolds number, lateral Reynolds number, thermal squeezing parameter, and the Hartmann number, respectively. They are defined as follows:

$$R_S = \frac{\rho h_o^2\omega}{\mu} \qquad R_L = \frac{\rho V_o h_o}{\mu}\left(\frac{h_o}{B}\right) \tag{20a,b}$$

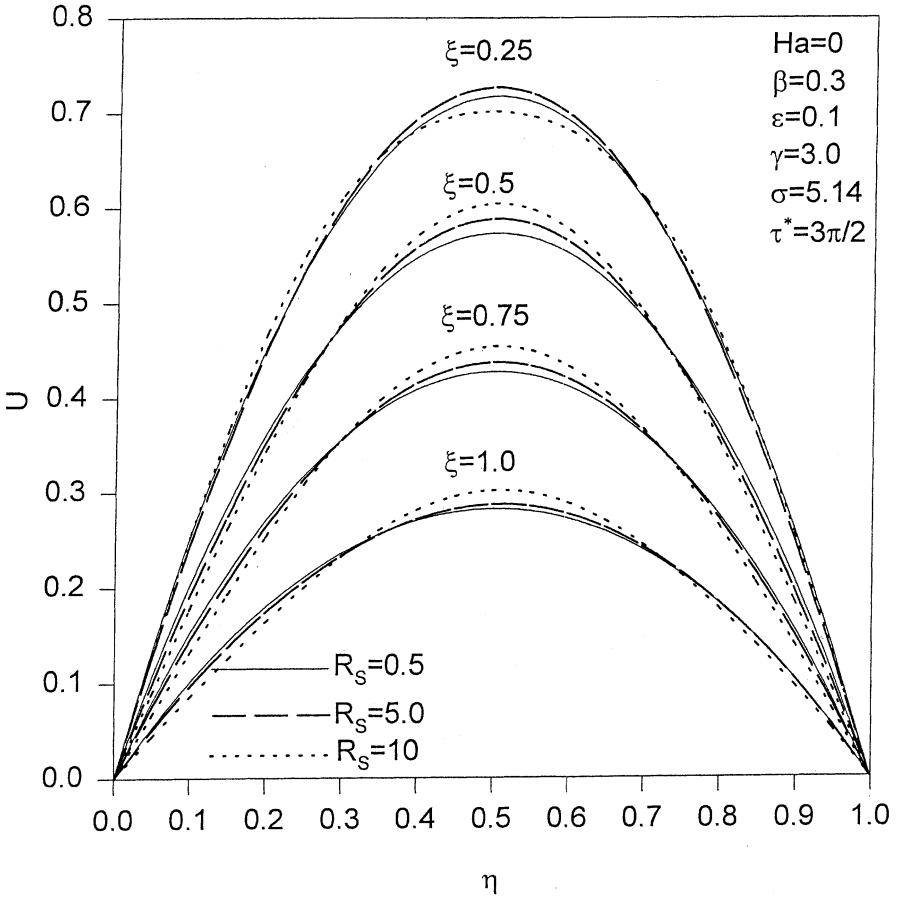

Figure 2. Effects of R_S on U profiles (low R_S).

$$P_S = R_S\, Pr \quad \text{Ha} = \sqrt{\frac{\sigma_m}{\mu}} B_m h_o \tag{20c, d}$$

where $\text{Pr} = \rho c_p \upsilon / k$ and it is the Prandtl number of the working fluid.

Dimensionless Boundary Conditions

The dimensionless boundary conditions for the flat thin film that will be implemented are

$$\Psi^*(0, Y, \tau) = \frac{V_o Y}{V_o + \omega B} \qquad \frac{\partial^2 \Psi^*(1, Y, \tau)}{\partial X^2} = 0$$

$$\Psi^*(X, 0, \tau) = 0 \qquad \Psi^*(X, H, \tau) = \frac{V_o H(\tau) - \omega B X \beta \sin(\gamma)}{V_o + \omega B}$$

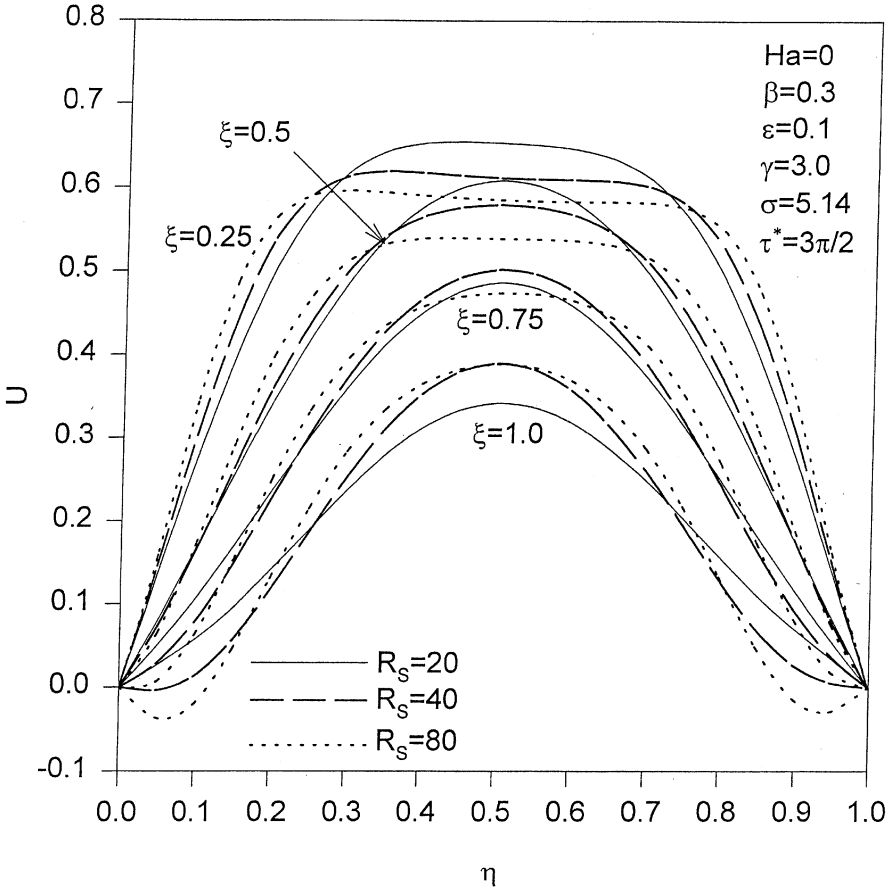

Figure 3. Effects of R_S on U profiles (high R_S).

$$\Psi^*(X, Y, 0) = 0$$

$$U(0, Y, \tau) = \frac{V_o}{(V_o + \omega B)} \quad U(X, 0, \tau) = 0 \quad U(X, H, \tau) = 0 \tag{21}$$

$$V(X, 0, \tau) = 0 \qquad V(X, H, \tau) = \frac{\omega B \gamma \beta \sin(\gamma \tau)}{V_o + \omega B}$$

$$\Omega^*(0, Y, \tau) = -\varepsilon^2 \frac{\partial^2 \Psi^*(0, Y, \tau)}{\partial X^2} \qquad \frac{\partial^2 \Omega^*(1, Y, \tau)}{\partial X^2} \cong 0 \tag{22}$$

$$\Omega^*(X, 0, \tau) = -\frac{\partial U(X, 0, \tau)}{\partial Y} \qquad \Omega^*(X, H, \tau) = -\frac{\partial U(X, H, \tau)}{\partial Y}$$

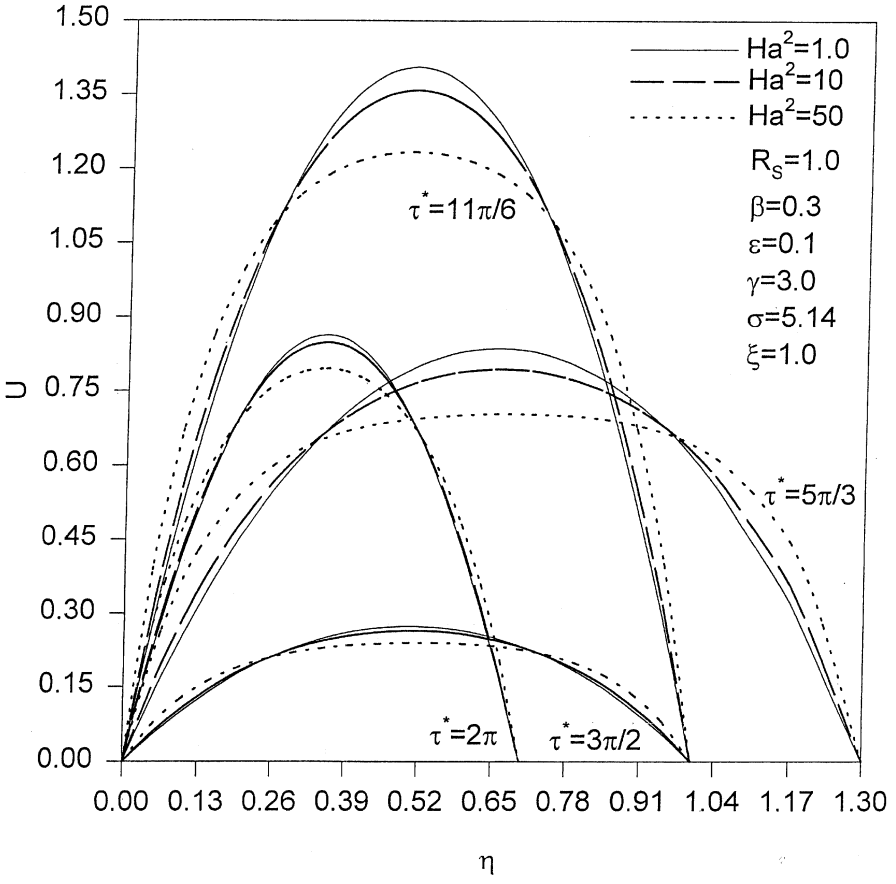

Figure 4. Effects of Ha on U.

$$\frac{\partial\theta(X,0,\tau)}{\partial Y} = -1 \qquad \frac{\partial\theta(X,H,\tau)}{\partial Y} = 0$$

$$\theta(X,Y,0) = 0 \qquad \theta(0,Y,\tau) = 0 \tag{23}$$

$$\frac{\partial\theta(1,Y,\tau)}{\partial X} \cong \frac{1}{(1+V_o/\omega B)U_m}\left(\frac{1}{P_S H} - \frac{\partial\theta_m(1,\tau)}{\partial\tau}\right)$$

where $H(\tau) = h/h_o$. θ_m is the dimensionless mean bulk temperature. It is equal to

$$\theta_m(X,\tau) = \frac{1}{U_m(X,\tau)H}\int_0^H U(X,Y,\tau)\theta(X,Y,\tau)dY \tag{24}$$

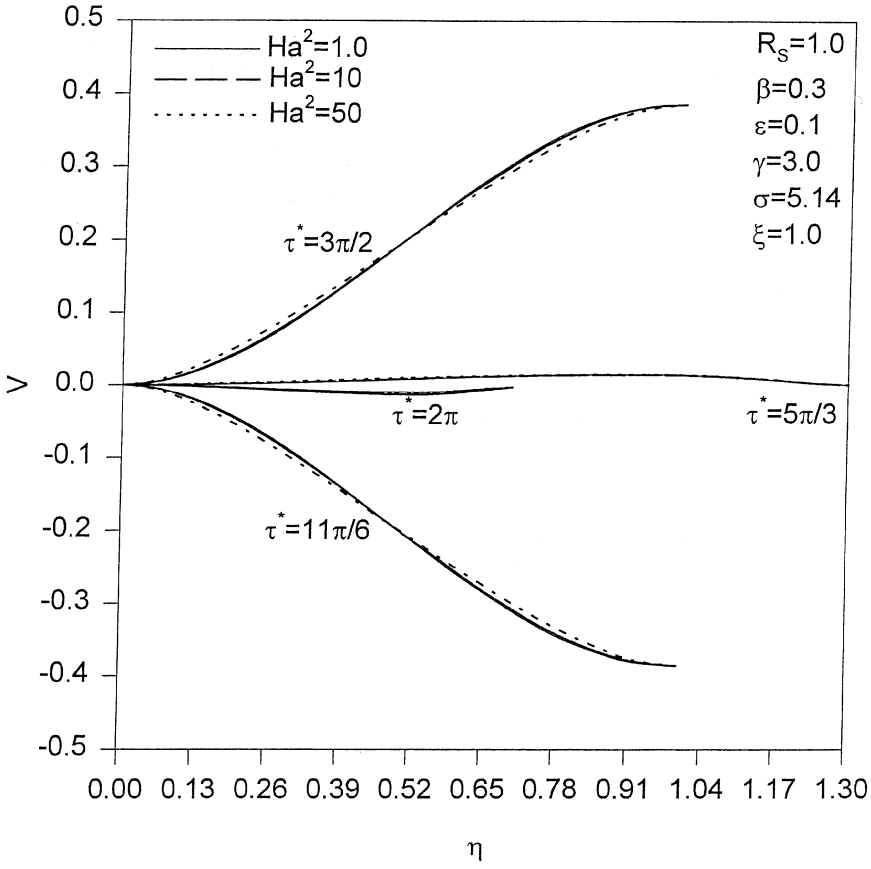

Figure 5. Effects of Ha on V.

It is suggested to express Eqs. (21) in terms of the following parameter:

$$\sigma = \frac{12}{1 + V_o/\omega B} \tag{25}$$

This number is called the squeezing number. Accordingly, Eq. (21) reduces to the following:

$$\Psi^*(0, Y, \tau) = \left(1 - \frac{\sigma}{12}\right) Y \qquad \frac{\partial^2 \Psi^*(1, Y, \tau)}{\partial X^2} = 0$$

$$\Psi^*(X, 0, \tau) = 0 \qquad \Psi^*(X, H, \tau) = \left(1 - \frac{\sigma}{12}\right) H(\tau) - \left(\frac{\sigma}{12}\right) X\beta\gamma \sin(\gamma t)$$

$$\Psi^*(X, Y, 0) = 0$$

$$U(0, Y, \tau) = \left(1 - \frac{\sigma}{12}\right) \quad U(X, 0, \tau) = 0 \quad U(X, H, \tau) = 0$$

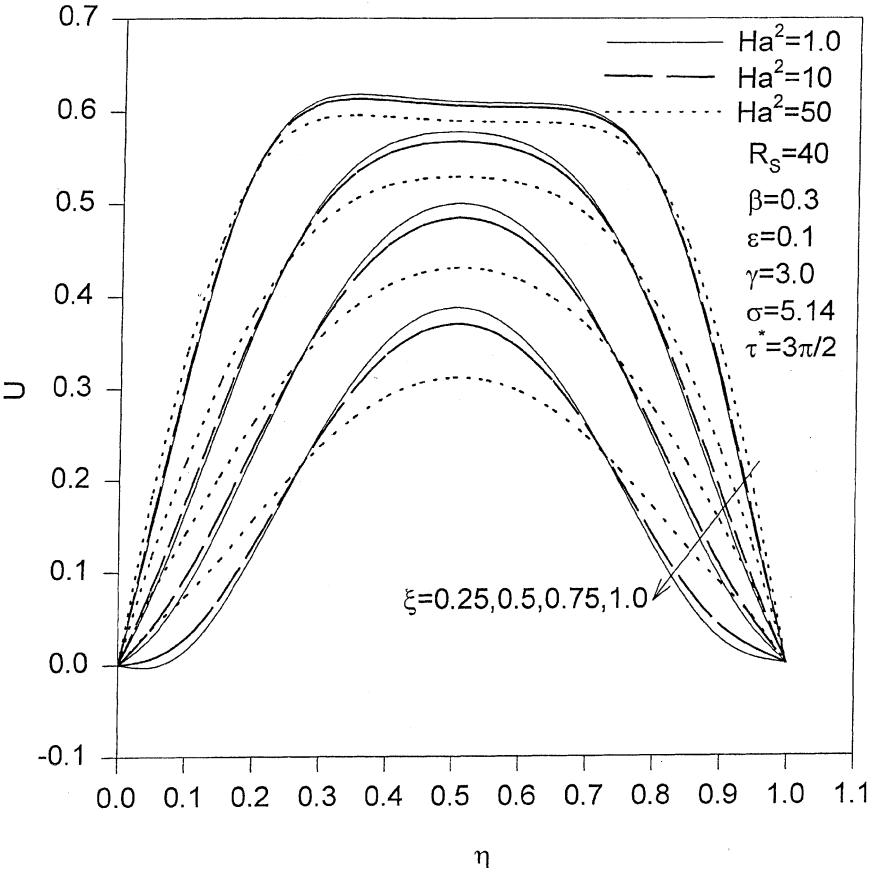

Figure 6. Effects of Ha on U profiles (high R_S).

$$V(X,0,\tau)=0 \qquad V(X,H,\tau)=\left(\frac{\sigma}{12}\right)\beta\gamma\sin(\gamma) \tag{26}$$

The appropriate dimensionless heat transfer parameter is the local Nusselt number defined at the lower plate, which is defined as follows:

$$\mathrm{Nu}_L(X,\tau)\equiv\frac{h_c h_o}{k}=\frac{1}{\theta(X,0,\tau)-\theta_m(X,\tau)} \tag{27}$$

where h_c is the convective heat transfer at the lower plate.

NUMERICAL ANALYSIS

Equations (17) through (19) are transformed from the X, Y, and τ domains into new computational domains, $\xi=X$, $\eta=Y/H$, and $\tau^*=\tau$. The transformed equations are

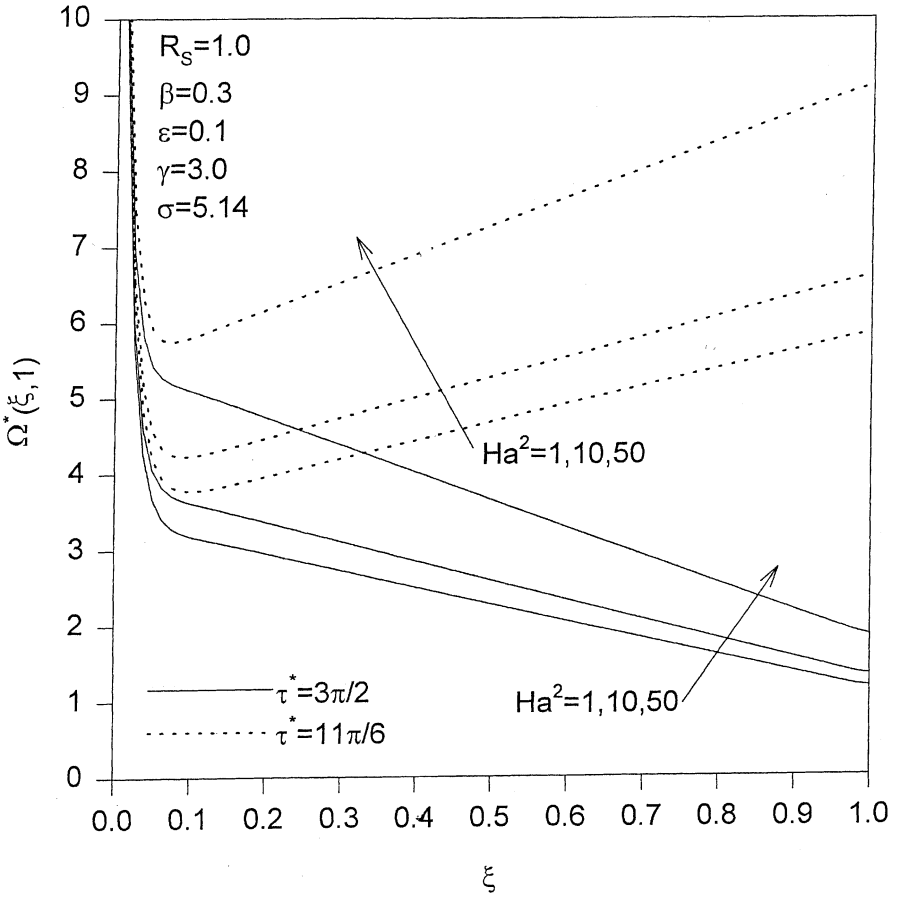

Figure 7. Effects of Ha on $\Omega^*(\xi, 1)$.

$$R_S H^2 \frac{\partial \Omega^*}{\partial \tau^*} + (R_S + R_L) U H^2 \frac{\partial \Omega^*}{\partial \xi} + \left[(R_S + R_L) V - R_S \eta \frac{dH}{d\tau^*} \right] H \frac{\partial \Omega^*}{\partial \eta} = \left(\varepsilon^2 H^2 \frac{\partial^2 \Omega^*}{\partial \xi^2} + \frac{\partial^2 \Omega^*}{\partial \eta^2} \right) - H_a^2 H^2 \Omega^* \tag{28}$$

$$\left(\varepsilon^2 H^2 \frac{\partial^2 \Psi^*}{\partial \xi^2} + \frac{\partial^2 \Psi^*}{\partial \eta^2} \right) = -\Omega^* H^2 \tag{29}$$

$$P_s \left(H^2 \frac{\partial \theta}{\partial \tau^*} + \left(1 + \frac{R_L}{R_S} \right) U H^2 \frac{\partial \theta}{\partial \xi} + \left[\left(1 + \frac{R_L}{R_S} \right) V - \eta \frac{dH}{d\tau^*} \right] H \frac{\partial \theta}{\partial \eta} \right) = \varepsilon^2 H^2 \frac{\partial^2 \theta}{\partial \xi^2} + \frac{\partial^2 \theta}{\partial \eta^2} \tag{30}$$

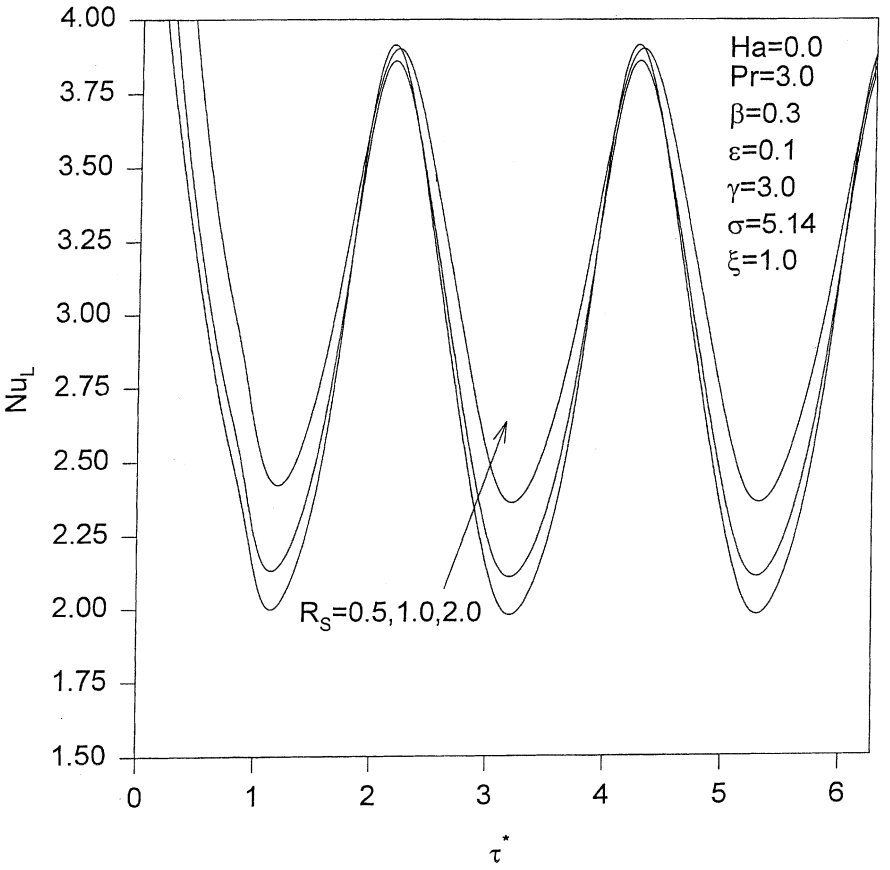

Figure 8. Effects of R_S on Nu_L.

Equations (28) and (30) were solved using an alternating direction implicit (ADI) method. Center differencing in space was used for discretizing the dimensionless vorticity and temperature differential terms, and forward differencing was used to approximate time differential terms. After each half step of time, Eq. (29) was solved using the method of successive overrelaxation (SOR).

The axial thermal condition at the exit, the last condition in Eq. (23), and the differential term $\partial\theta_m(1,\tau)/\partial\tau$ are reducible to $\partial\theta_m(1,\tau^*)/\partial\tau^*$, which in turn can be approximated by $\partial\theta(1,\eta,\tau^*)/\partial\tau^*$ because the thickness of the used films is small. Further the dimensionless velocities in Eq. (28) as well as the dimensionless vorticity at the plates of the thin film, seen in Eqs. (22), were calculated initially at previous half time steps, and they are corrected later using an iterative procedure for Eqs. (28) and (29) every half time step. The dimensionless velocities in the reduced energy equation were evaluated at the present time step.

The value of γ in Eq. (1) was chosen to be 3.0 in the developed figures. Note that other values of γ will result in similar physical behavior. Based on extensive numerical experimentation, the values of 0.0125, 0.05, 0.001, and 10^{-5} were chosen

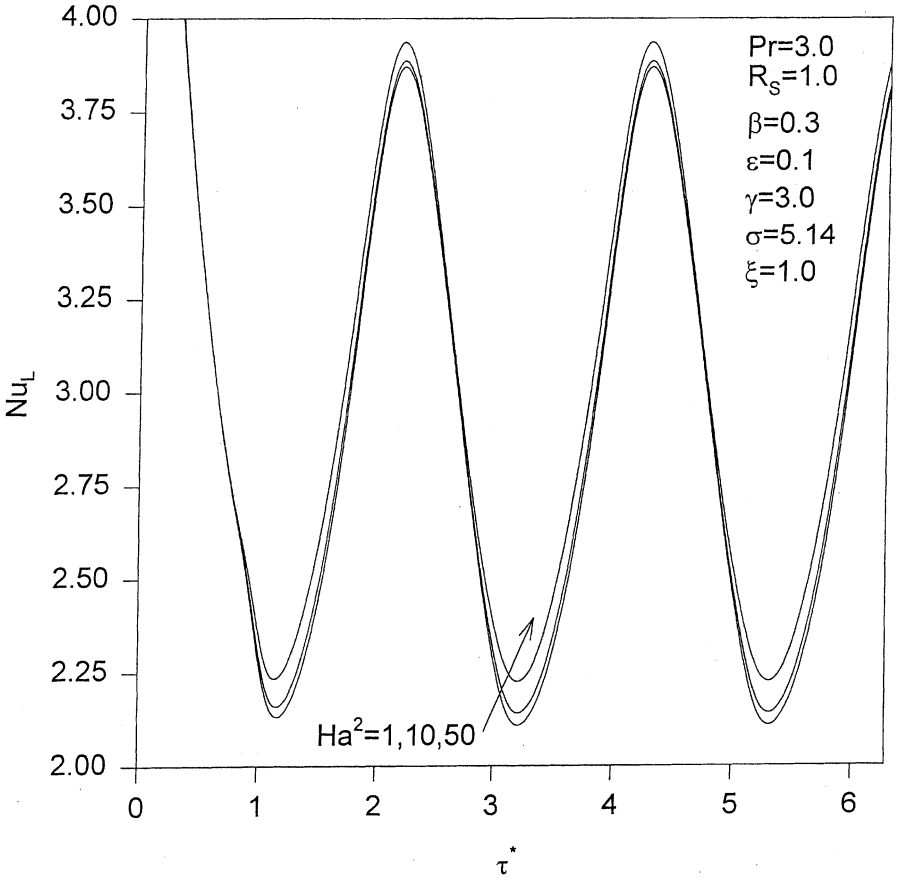

Figure 9. Effects of Ha on Nu_L.

for $\Delta\xi$, $\Delta\eta$, $\Delta\tau^*$, and the maximum error for stream functions in Eq. (28), respectively. These values resulted in grid and time independence solutions.

DISCUSSION OF RESULTS

Figures 2 and 3 show the effects of the squeezing Reynolds number R_S on the axial velocity profiles at $\tau^* = 3\pi/2$ when the upper plate reaches its maximum speed in a relief stage. It is noticed that inlet effects convect large distances from the inlet as R_S increases. This is shown in Figure 3, where the core of the velocity profile becomes flatter at $\xi = 0.25$ as R_S increases. Further, it is observed that the vorticity at both boundaries decreases as R_S increases while it increases during squeezing stages. Flow instabilities start to appear at large R_S values as shown in Figure 3. It is worth noting that the values of R_S can be increased either by increasing the film thickness or by decreasing the fluid viscosity and that the frequency of the disturbance is kept constant since the squeezing number σ is kept constant.

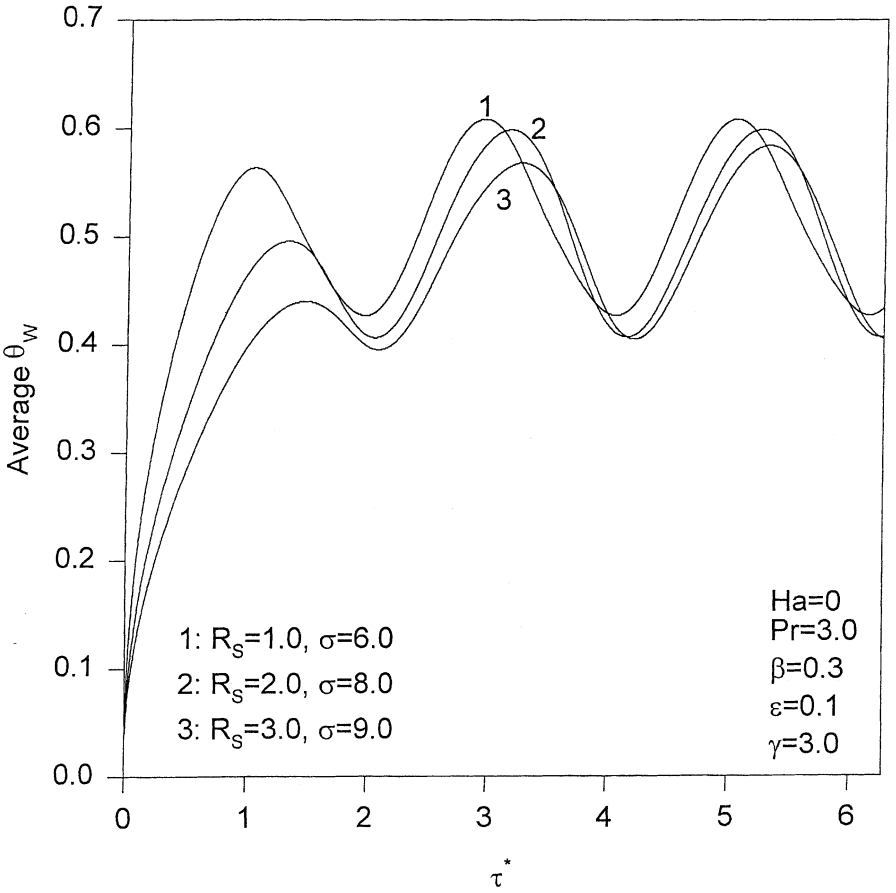

Figure 10. Effects of ω on average θ_W.

Figures 4 and 5 show the influence of the square of Hartmann number Ha^2 on dimensionless axial and normal velocity profiles at the exit, respectively. Imposition of a magnetic field normal to axial flow produces a resistive force. This force is called the Lorentz force, which has a tendency to suppress the movement of the fluid. This suppression is noticed in Figure 4, where the core of the velocity profiles decreases as Ha increases. However the uniformity of the velocity profiles increases as Ha increases. With regards to normal velocities, increases in the values of Ha increase the variations in the dimensionless velocity profiles near the lower plate, yet these variations are small compared with the variations in the values of Ha. This can be noticed from Figure 5.

Figure 6 shows the effects of Ha on axial dimensionless velocity profiles for a relatively large value of squeezing Reynolds number R_S at $\tau^* = 3\pi/2$. The increased uniformity in the velocity profile that resulted from the imposition of the normal magnetic field caused the fluid near the lower plate to have enough kinetic energy to overcome the instabilities due to increases in the pressure during relief stages.

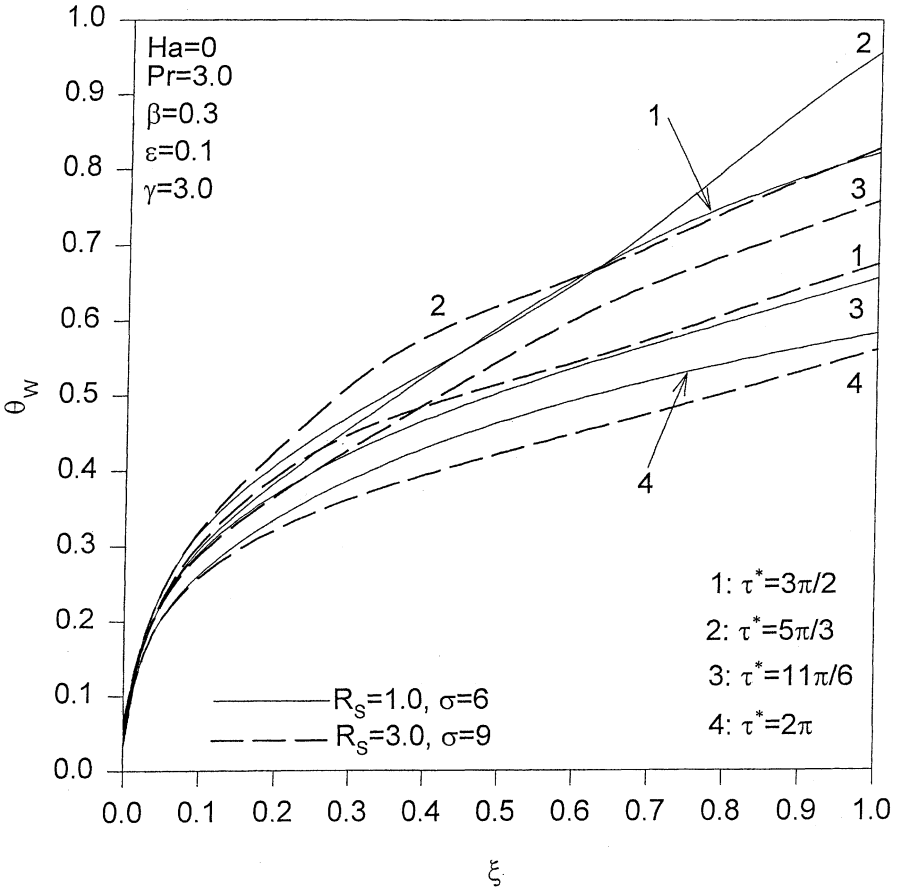

Figure 11. Effects of ω on axial distribution θ_W.

Figure 7 describes the effects of Ha on the axial distribution of the vorticity evaluated at the top surface $\Omega^*(\xi,1)$ of the thin film at two different times. It is noticed that $\Omega^*(\xi,1)$ increases as Ha increases due to increases in the Lorentz resistive force. This implies that surface stresses increase as Ha increases since the wall shear stress is proportional to $\Omega^*(\xi,1)$. Note that wall shear stresses increase as dimensionless axial distance ξ increases during squeezing periods while they decrease during relief stages as seen in Figure 7. While a magnetic field resulted in a reduction in flow instabilities inside the thin film at large R_S values, it introduced larger flow resistances. As such, more pumping power is required to maintain a constant average velocity or a constant flow rate at the inlet.

Figure 8 represents the effects of R_S on the history of the local Nusselt number at the lower plate Nu_L at the exit of the thin film. Variations in Nusselt numbers are significant in relief stages where the fluid inertia, thermal transient effects, and thermal convections are maximum due to increases in flow rates as the volume inside the thin film increases. Figure 9 illustrates the effects of Ha on the Nusselt number. Increasing the magnetic strength when Ha increases results in increasing the flow

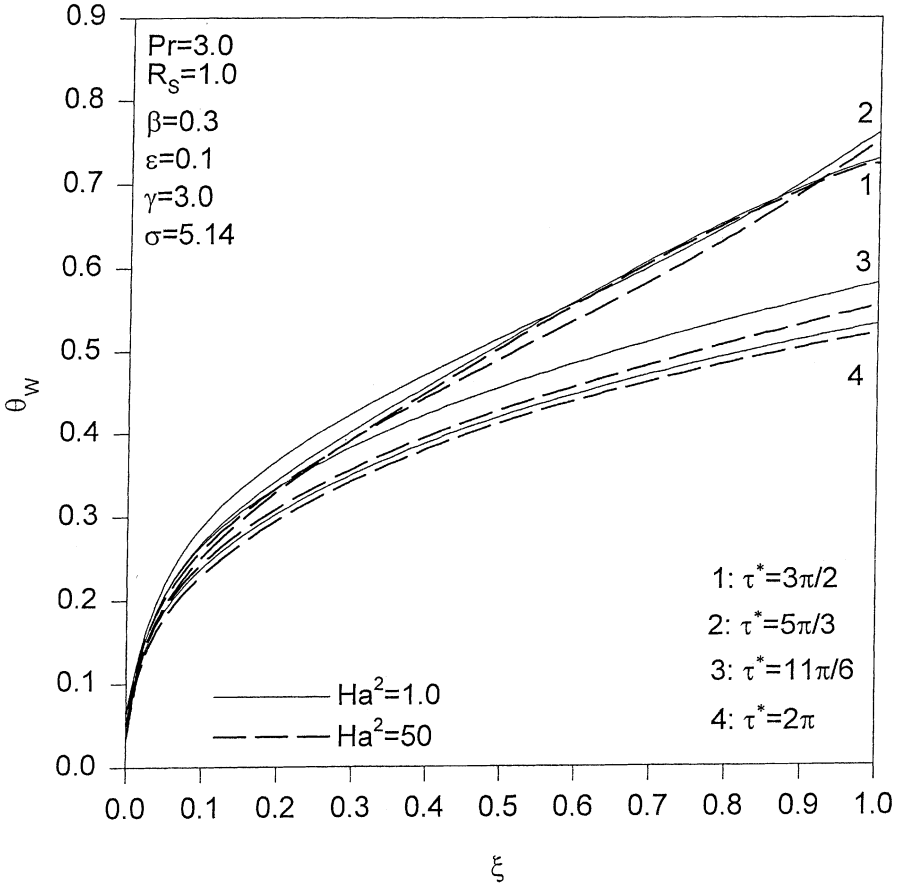

Figure 12. Effects of Ha on axial distribution θ_W.

near the plates of the thin film, resulting in an increasing convective heat transfer coefficient at the lower plate; thus Nusselt numbers increase as Ha increases for thin films with similar average flow rates.

Figure 10 illustrates the effects of varying the squeezing frequency on the average lower plate temperature θ_W. The reference frequency for cases 2 and 3 is twice and three times the frequency of case 1, respectively. It is noticed that the average θ_W and its fluctuations decrease as the squeezing frequency increases since this causes enhancements in thermal convections. Further, a phase shift is recognized between the different plots due to increases in both inertia and thermal transient effects as squeezing frequency increases. The axial behavior of the wall temperature θ_W under two different squeezing frequencies is shown in Figure 11. When the frequency is increased by a factor of three, the fluctuations are reduced as shown in Figure 11. This is because changes that happen to the flow occur at a fast rate as the frequency increases, causing inefficient heat diffusion. In the presence of a magnetic field normal to the flow direction, increases in Ha cause increases in a convective heat transfer coefficient, which decreases the lower plate temperature as shown in Figure 12.

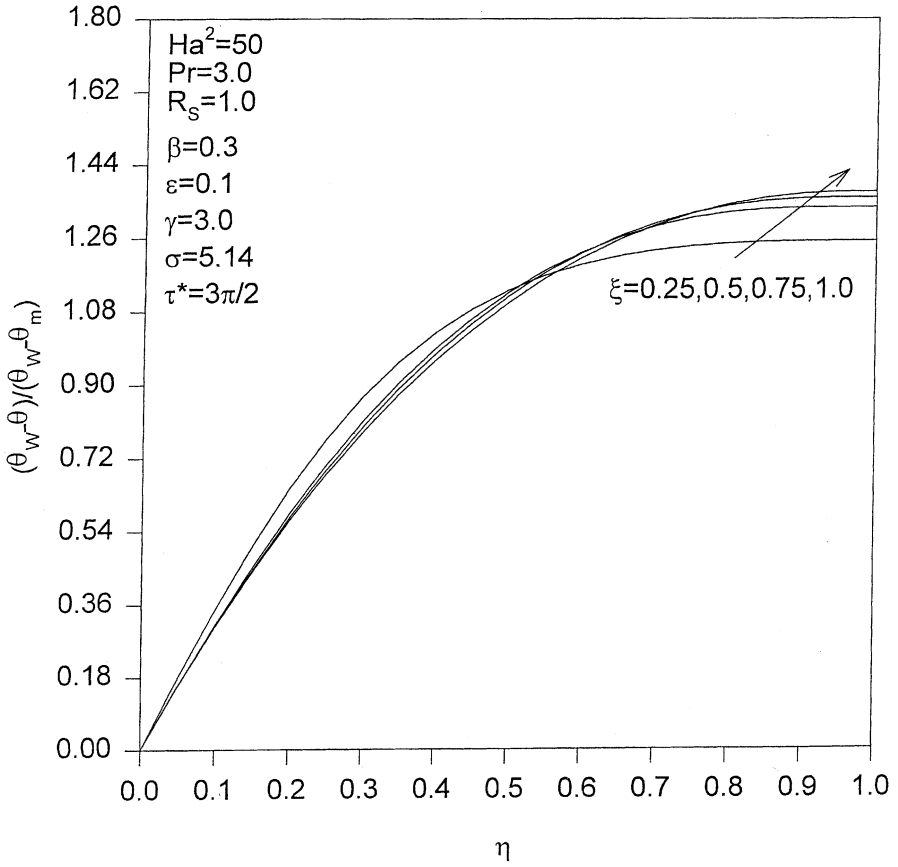

Figure 13. Axial development of temperature profiles.

Figure 13 displays the axial development of the dimensionless temperature profile at the maximum relief velocity. We can see from this figure that the axial gradient of this newly defined dimensionless temperature reaches almost negligible values far from the inlet as shown in Figure 13. Consequently, the following can be considered as the exit thermal boundary condition inside squeezed thin films, and it was utilized in developing Figures 10 and 11 to avoid singularities associated with the exit thermal condition during backflows:

$$\frac{\partial}{\partial X}\left(\frac{\theta_w - \theta}{\theta_w - \theta_m}\right) = 0 \tag{31}$$

Figure 14 shows the effects of the squeezing number σ on the Nusselt number Nu_L. It is noticed that the Nusselt number is almost unaffected by the squeezing number, especially at larger values of σ. That is because the flow reaches its thermally fully developed conditions at shorter distances for larger σ values than for smaller σ values. Accordingly, the Nusselt number is mainly affected by σ only if the inlet velocity is much greater than the maximum induced axial squeezed velocity.

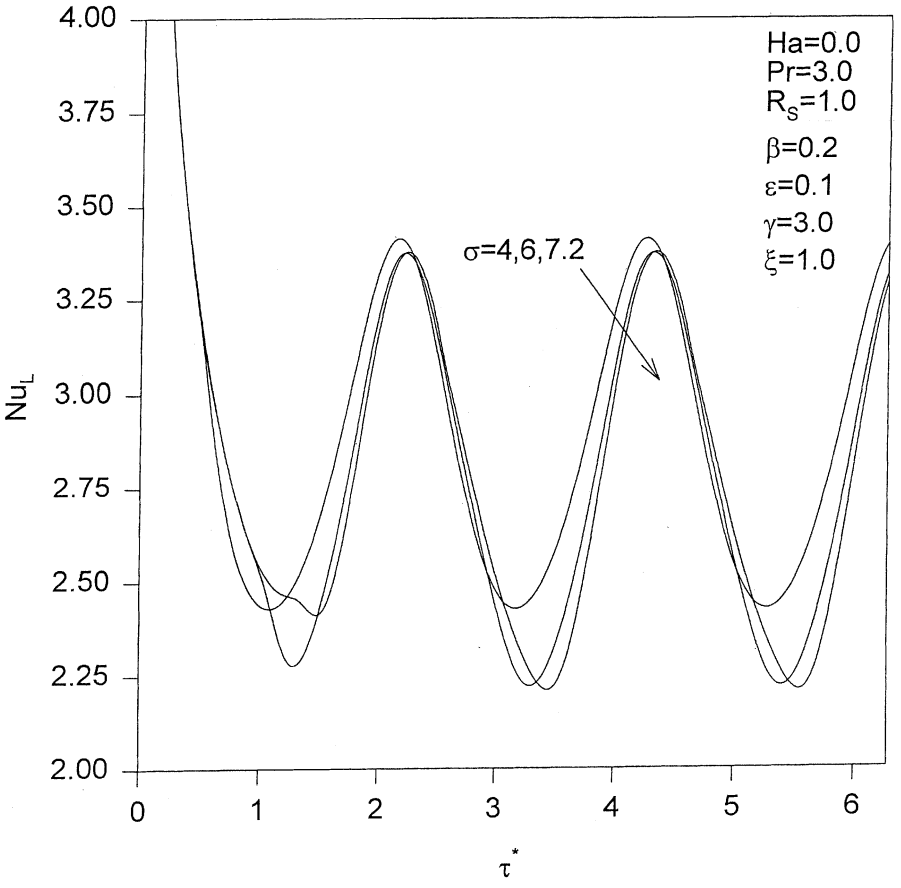

Figure 14. Effects of σ on Nu_L.

Based on the presented results, application of the magnetic field is recommended in order to reduce flow instabilities. These can be due internal disturbances such as thin films having pulsating flows or due to external disturbances such as for oscillatory squeezed thin films. Further, isolating the existing thin films against vibrations with a lower squeezing frequency will produce a more thermally stable thin film.

CONCLUSIONS

The flow and heat transfer effects during the squeezing and relief stages for an incompressible thin film at a wide range of squeezing Reynolds numbers have been considered in the presence of a magnetic field. Although flow inside thin films has been studied in the past, the heat transfer characteristics of thin films with oscillating squeezing boundaries have received less attention especially in the presence of a magnetic field. In this study, the proper voticity stream function formulations and the energy equation were nondimensionalized. It was found that flow instabilities

increase as the squeezing Reynolds number increases. These instabilities were found to decrease as the Hartmann number increases. In addition, the average wall temperature and the corresponding fluctuations in this temperature were found to decrease as the squeezing frequency increases. The Nusselt number was found to be affected by variations in the squeezing Reynolds number, and also the Nusselt number was found to increase as the Hartmann number increases.

REFERENCES

1. N. V. Lavrik, C. A. Tipple, M. J. Sepaniak, and D. Datskos, Gold Nano-Structure for Transduction of Biomolecular Interactions into Micrometer Scale Movements, *Biomedical Microdevices*, vol. 3, no.1, pp. 35–44, 2001.
2. W. E. Langlois, Isothermal Squeeze Films, *Quarterly of Applied Math.*, vol. XX, pp. 131–150, 1962.
3. S. H. Damodaran, G. W. Rankin, and C. Zhang, Effect of a Moving Boundary on Pulsatile Flow of Incompressible Fluid in a Tube, *Computational Mechanics*, vol. 23, pp. 20–32, 1999.
4. R. C. Bhattacharjee, N. C. Das, and A. K. Pal, Analysis of an Unsteady Squeezing Flow of Dusty Fluids, *Tribology International*, vol. 32, pp. 427–434, 1999.
5. E. A. Hamza, Unsteady Flow Between Two Disks with Heat Transfer in the Presence of a Magnetic Field, *J. Phys. D: Appl. Phys.*, vol. 25, pp. 1425–1431, 1992.
6. S. Bhattacharyya, A. Pal, and G. Nath, Unsteady Flow and Heat Transfer Between Rotating Coaxial Disks, *Numerical Heat Transfer, Part A*, vol. 30, pp. 519–532, 1996.
7. B. Debbaut, Non-Isothermal and Viscoelastic Effects in the Squeeze Flow Between Infinite Plates, *J. Non-Newtonian Fluid Mech.*, vol. 98, pp. 15–31, 2001.
8. A.–R. A. Khaled and K. Vafai, Non-Isothermal Characterization of Thin Film Oscillating Bearings, *Numerical Heat Transfer: Part A*, vol. 41, pp. 451–467, 2002.
9. A. J. Chamkha, Unsteady Laminar Hydromagnetic Flow and Heat Transfer in Porous Channels with Temperature-Dependent Properties, *International Journal of Numerical Methods for Heat & Fluid Flow*, vol. 11, pp. 430–448, 2001.
10. S. Bhattacharyya and A. Pal, Unsteady MHD Squeezing Flow Between Two Rotating Discs, *Mechanics Research Communications*, vol. 24, pp. 615–623, 1997.